Journal of Dental Sciences 18 (2023) 73–80

Available online at www.sciencedirect.com

ScienceDirect

journal homepage: www.e-jds.com

Original Article

Surface modification of zirconia ceramics through cold plasma treatment and the graft polymerization of biomolecules

Kuo-Ning Ho [a], Liang-Wei Chen [b], Tzong-Fu Kuo [c], Ko-Shao Chen [d], Sheng-Yang Lee [a,e**], Sea-Fue Wang [b*]

[a] School of Dentistry, College of Oral Medicine, Taipei Medical University, Taipei, Taiwan
[b] Department of Materials and Mineral Resources Engineering, National Taipei University of Technology, Taipei, Taiwan
[c] School of Veterinary Medicine, National Taiwan University, Taipei, Taiwan
[d] Department of Mechanical and Materials Engineering, Tatung University, Taipei, Taiwan
[e] Department of Dentistry, Wan-Fang Medical Center, Taipei Medical University, Taipei, Taiwan

Received 15 June 2022; Final revision received 16 June 2022
Available online 31 July 2022

KEYWORDS
Zirconia;
Cold plasma treatment;
Graft polymerization;
Biomolecules;
Biocompatibility

Background/purpose: Although zirconia ceramics were highly versatile as dental implants, their long-term presence in the human body may slow down healing and impede cell growth in the past. To enhance the cytocompatibility of zirconia ceramics, surface activation modification was used to immobilize biopolymers such that a biomimetic environment was created.
Materials and methods: Hexamethyldisilazane thin films were deposited onto the surface of inorganic zirconia through cold plasma treatment under various power and deposition time settings to form an organosilane interface layer. Next, oxygen plasma treatment was performed to activate the free radicals on the surface. Subsequently, ultraviolet light was employed to graft and polymerize acrylic acid for generating carboxyl groups on the surface. This was followed by a condensation reaction with biopolymers (chitosan, chitosan/poly-γ-glutamic acid, and gelatin).
Results: Under a 20-min deposition time at 40 W and 150 mTorr, the thin films had a maximum graft density of 2.1 mg/cm^2. MG-63 cells (human osteosarcoma cells) were employed to evaluate cell compatibility. Chitosan and chitosan/poly-γ-glutamic acid promoted the compatibility of MG-63 cells (a human osteosarcoma cell line) with zirconia ceramics, whereas gelatin reduced this compatibility.

* Corresponding author.Department of Materials and Mineral Resources Engineering, National Taipei University of Technology, No.1, Sec 3., Chung-Hsiao East Rd., Taipei 10617, Taiwan.
** Corresponding author.School of Dentistry, College of Oral Medicine, Taipei Medical University, No. 250, Wu-Hsing Street, Taipei 11031, Taiwan.
E-mail addresses: seanlee@tmu.edu.tw (S.-Y. Lee), sfwang@ntut.edu.tw (S.-F. Wang).

https://doi.org/10.1016/j.jds.2022.06.007

Conclusion: The findings confirm that cold plasma treatment and graft polymerization can promote the immobilization of biomolecules and improve the biocompatibility of zirconia ceramics. This approach can be applied to the modification of zirconia ceramic implants.

Introduction

Biomedical materials made of metal or ceramics have seen widespread use in numerous fields. Metal has long been employed as an implant material. However, metal implants are ill-suited for individuals with metal hypersensitivity. Moreover, they are aesthetically unappealing, which becomes a concern in cases of marginal bone resorption and gingival recession.[1] Consequently, ceramic materials, which are bioinert, have attracted scholarly attention as a preferred alternative.[2,3]

Zirconia-based ceramics are valuable biomedical materials, with a flexural strength twice that of aluminum oxide.[4,5] As dental implants, zirconia ceramics facilitate osseointegration[6,7] and possess the qualities required of all biomedical materials; they are nontoxic, noncarcinogenic, hypoallergenic, noninflammatory, biocompatible, biofunctional, aesthetically pleasing, corrosion resistant, and heat resistant. Thus, zirconia can replace titanium as a material for dental implants.[8–10]

Zirconia ceramics are bioinert and inorganic, but they are also brittle, which limits their biomedical applications. In one study, researchers overcame this problem by manipulating the processing parameters of zirconia ceramics.[11] Although zirconia ceramics are highly versatile as dental implants, their long-term presence in the human body may slow healing and impede cell growth.[12] To enhance inorganic implants' biocompatibility with the human body, studies have conducted animal experiments involving surface modification with hydrofluoric acid etching, successfully increasing the osseointegration stability of zirconia ceramics.[13,14] Other investigations have reported that material surface processing performed in cell culture with cold plasma reduced the contact angle with the material surface, thereby improving osteoblast attachment and growth.[15,16]

For the human body, a zirconia implant is a foreign object. To accelerate cell attachment, fixing biomolecules onto the surface of zirconia ceramics for the creation of a biomimetic environment may be a feasible approach. This surface modification process promotes greater biocompatibility between the implant material and the human body.

Few studies have sought to determine the biomolecules most suitable for the surface modification of inorganic materials or the plasma power and time required for their processing. To identify the optimal conditions for surface modification, we compared hexamethyldisilazane films of various thicknesses, which underwent deposition under various plasma power and processing time settings. Furthermore, we examined the performance of various biomolecules. In addition, we observed the proliferation of MG-63 cells, human osteoblast-like cells, to provide a reference for future applications of zirconia ceramic surface modification.

Materials and methods

Substrate preparation

In the laboratory, we fabricated ceramic substrates containing 3 mol% yttria-stabilized zirconia in two sizes: 10 mm × 10 mm × 1 mm for surface modification and 8.5 mm (diameter) × 1 mm (thickness) for cell culture.

Cold plasma surface deposition

The equipment setup for cold plasma surface deposition is illustrated in Fig. 1(a). The experiment was powered by a generator with a radiofrequency of 13.56 MHz. The process is described as follows. The air in the reaction chamber was first expelled using a rotary pump, making the reaction chamber reach a vacuum of <30 mTorr. The difference in air pressure enabled the introduction of hexamethyldisilazane monomers (purity >98%, molar mass [MW] = 161.39 g/mol; Fluka Chemie GmbH, Buchs, Switzerland) maintained at 150 mTorr. After the air pressure in the reaction chamber stabilized, plasma deposition was performed on the substrates at processing powers of 20, 40, and 60 W for 1, 5, 10, 20, and 30 min.

Cold plasma–activated surface processing

The equipment setup is illustrated in Fig. 1(b). The same generator employed in cold plasma surface deposition was employed, and the process was as follows. The air in the reaction chamber was first expelled using a rotary pump, making the reaction chamber reach a vacuum of <30 mTorr. The difference in air pressure enabled the introduction of oxygen (purity >99%; San Fu Chemical Co., Taipei, Taiwan) maintained at 50 mTorr. After the air pressure in the reaction chamber stabilized, O_2 plasma was activated on the substrates, which had been coated with a hexamethyldisilazane film, under a processing power of 100 W for 5 min. Thus, the functional groups on the substrate surface were activated.

Preparation of the graft polymerization solution

The solution used for the graft polymerization of polymeric monomers was an acrylic acid (AAc) solution (10 wt%; purity >98%, MW = 72.06 g/mol; Wako Pure Chemical Corp., Osaka, Japan). To this solution, ammonium persulfate

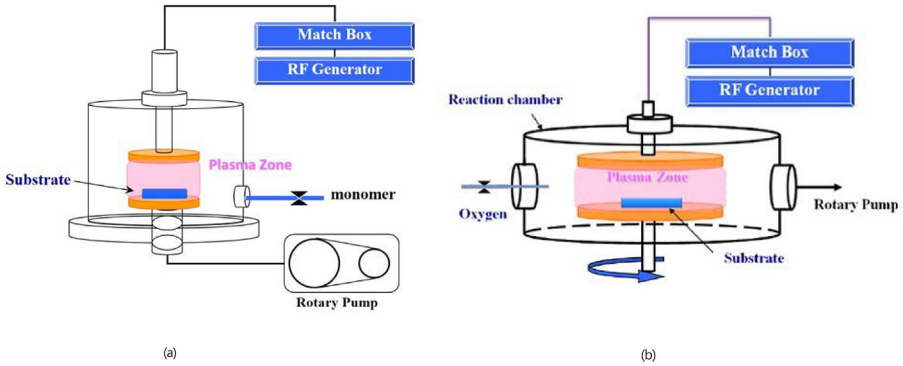

Fig. 1 Equipment setup for cold plasma surface deposition. (b) Equipment setup for O_2 plasma surface deposition.

(MW = 228.20 g/mol; Wako Pure Chemical Corp.) and vitamin B (MW = 376.37 g/mol; MilliporeSigma, St. Louis, MO, USA) was added to serve as initiator and antioxidant, respectively, in graft polymerization. The oxygen in the solution was removed by passing N_2 gas through the solution.

Preparation of the surface cross-linking displacement solution

Carboxyl groups (-COOH), 1-ethyl-3-(3-dimethylaminopropyl) carbodiimide hydrochloride (EDC, MW = 191.70 g/mol; MilliporeSigma), and N-hydroxysuccinimide (NHS, purity >98%, MW = 115.09 g/mol; MilliporeSigma) solutions (0.01 M) were prepared and mixed at a 1:1 ratio in 0.1 M 2-(N-morpholino) ethanesulfonic acid (MES) buffer (MES sodium salt, MW = 217.2 g/mol; MilliporeSigma).

Surface graft polymerization

Cold plasma—treated substrates were submerged in the prepared AAc solution and placed under ultraviolet (UV) light (1000 W, wavelength = 365 nm) for 30 min to induce the graft polymerization of AAc monomers onto the substrate surface. Cooling water was introduced to prevent violent temperature changes. Following graft polymerization, the substrates were rinsed with deionized water for 15 min to remove AAc monomers that were uninvolved in the reaction. The substrates were then left to dry at room temperature.

Surface cross-linking and immobilization of biomolecules

A. Fixing chitosan and gelatin biomolecule films

The substrates that had undergone graft polymerization were submerged in the EDC/NHS solution and maintained at 4 °C for 24 h. The substrates were then removed from the EDC/NHS solution, submerged in a chitosan solution (2 wt%, 75%—80% deacetylation, medium molecular weight; MilliporeSigma) or a gelatin solution (1 wt%; MilliporeSigma) and maintained at 4 °C for 24 h to allow the biomolecules to be fixed in place.

B. Fixing a chitosan/poly-γ-glutamic acid biomolecule film

The substrates that had undergone graft polymerization were submerged in the EDC/NHS solution and maintained at 4 °C for 24 h before being removed from the EDC/NHS solution. Next, the substrates were submerged in a chitosan solution (1 wt%) and maintained at 4 °C for 24 h. Subsequently, they were submerged in a solution prepared by mixing poly-γ-glutamic acid (γ-PGA; MW = 100,000—300,000 g/mol; Vedan Enterprise Corp., Taichung, Taiwan) with the EDC/NHS solution at a 1:1 ratio. The substrates were then maintained at 4 °C for 24 h. Fig. 2 presents a schematic of a substrate after it was subjected to surface modification.

Graft density and immobilization density

We measured the weight of the substrates in the initial untreated state, following graft polymerization with AAc molecules, and following biomolecule immobilization. The mean weight of the three substrates was determined. The following equations were applied to the calculation of graft density D_G and immobilization density D_I.

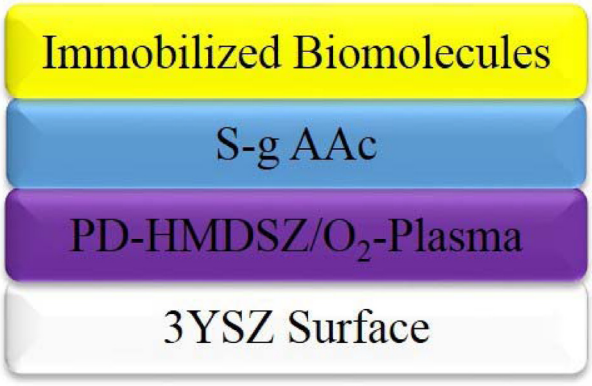

Fig. 2 Schematic of a substrate after surface modification.

$$D_G\,(mg/cm^2) = \frac{(W_{AAc} - W_i)}{\text{sample area}}$$

$$D_I\,(mg/cm^2) = \frac{(W_I - W_{AAc})}{\text{sample area}}$$

W_i: initial weight (mg).

W_{AAc}: dry weight following graft polymerization with AAc molecules (mg).

W_I: dry weight following biomolecule immobilization (mg).

Ellipsometry analysis of film thickness

We conducted an ellipsometry analysis of film thickness, which involves using the polarization of light beams penetrating or reflecting off an interface or thin film to measure the thickness of one or multiple layers of film. This highly precise technique enables the measurement of films ranging in thickness from subnanometers to micrometers. Furthermore, it is noninvasive and noncontact.

Analysis of surface hydrophilicity—hydrophobicity

An analysis of surface hydrophilicity—hydrophobicity was conducted through the sessile drop method. Using a probe, a droplet of deionized water (approximately 1.0 μL) was gently moved onto a substrate. After the probe was removed, a video-based optical contact angle meter (Model 100SB, Sindatek Instrument Co., Ltd, New Taipei City, Taiwan) was employed to measure the contact angle of the droplet. The mean value of three points on each substrate was considered. The results were analyzed to determine changes in surface hydrophilicity.

Fourier-transform infrared spectroscopy of changes in surface functional groups

Fourier-transform infrared spectroscopy (FTIR) was performed for surface functional group analysis under the following settings: scan number = 128, resolution = 32 cm^{-1}, and spectral range = 600—4000 cm^{-1}. The background value was set to air, and the samples were scanned separately on the stage. The obtained spectrograms were compared with those in the literature and databases to identify the functional groups the characteristic peaks represented. Furthermore, changes in functional groups in each step of the experiment were documented.

Cell viability analysis through the 3-(4,5-dimethylthiazol-2-yl)-2,5-diphenyltetrazolium bromide assay

MG-63 cells were used for cell compatibility testing. Substrates were placed in a polystyrene 24-well cell culture plate, submerged in alcohol, and sterilized under UV light for 24 h. Each substrate was seeded with 5×10^4 cells, incubated under 5% CO_2 at 37 °C for 24 h, and then washed with 1 × phosphate-buffered saline to remove necrotic cells. Subsequently, 500 μL of 3-(4,5-dimethylthiazol-2-yl)-2,5-diphenyltetrazolium bromide (MTT) solution was added, and the cells were incubated for 4 h to induce cell—MTT interaction. Finally, the cultured solution was collected and mixed with 1 mL of dimethyl sulfoxide solution, shaken for 30 min at 150 rpm, and subjected to the enzyme-linked immunosorbent assay at a wavelength of 570 nm to measure light absorbance. Cell compatibility was determined according to the light absorbance value.

Statistical analysis

All data are expressed as means ± standard deviations. One-way analysis of variance was performed, with the level of significance set at $P < 0.05$.

Results

Graft density and immobilization density

Table 1 presents the graft density values, which were calculated on the basis of the weight differences resulting from variations in processing power and deposition time to which the hexamethyldisilazane films were subjected. As shown in Fig. 3, in the 20-W and 40-W groups, the graft density increased as the deposition time (i.e., the cold plasma treatment time) increased from 1 to 30 min. However, when the deposition time reached 30 min, the graft density declined sharply. In the 60-W group, the graft density peaked when the deposition time reached 5 min. From that point onward, as the deposition time increased, the graft density decreased considerably.

The 20-W and 40-W groups under 20-min deposition (designated as PD-H 20-20 and PD-H 40-20, respectively), which exhibited substantial changes in graft density at the time point, along with the 60-W group (designated as PD-H 60-20 and serving as the control) at the same time point, were used to calculate the immobilization density of chitosan, chitosan/γ-PGA, and gelatin (Table 2). In all groups, immobilization density changed considerably. The

Table 1 Graft density under the effect of cold plasma processing power and deposition time.

Graft density (mg/cm^2)				
PD-H 20-1	PD-H 20-5	PD-H 20-10	PD-H 20-20	PD-H 20-30
0.2 ± 0.1	0.1 ± 0.1	0.1 ± 0.1	0.6 ± 0.3	0.6 ± 0.2
PD-H 40-1	PD-H 40-5	PD-H 40-10	PD-H 40-20	PD-H 40-30
0.2 ± 0.2	0.1 ± 0.1	0.2 ± 0.1	2.1 ± 0.4	0.5 ± 0.1
PD-H 60-1	PD-H 60-5	PD-H 60-10	PD-H 60-20	PD-H 60-30
0.1 ± 0.1	1.3 ± 0.4	0.5 ± 0.1	0.5 ± 0.1	0.2 ± 0.1

Graft density, calculated on the weight differences of hexamethyldisilazane films from variations in processing power and deposition time. PD, processing power; H, deposition time. Processing power of cold plasma treats were 20, 40, 60 W. Deposition time of hexamethyldisilazane films were 1 min, 5 min, 10 min, 20 min, 30 min.

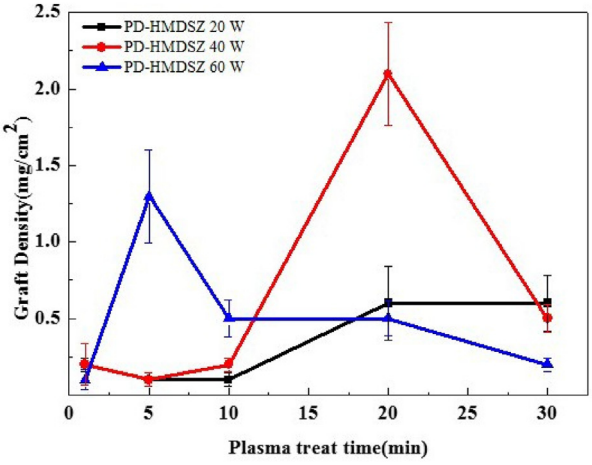

Fig. 3 Effect of hexamethyldisilazane film deposition time on graft density.

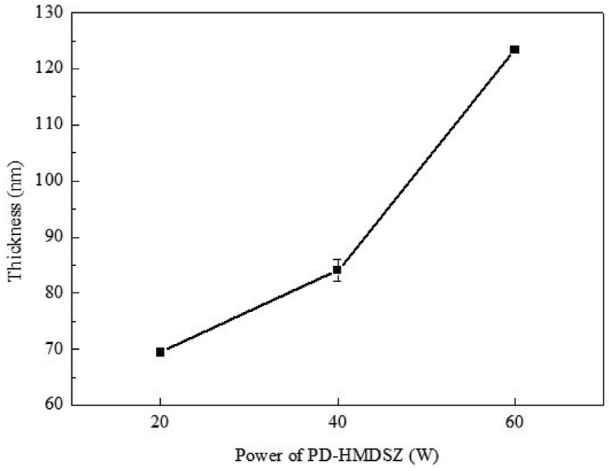

Fig. 4 Effect of processing power on film thickness under a fixed deposition time.

Table 2 Graft density and immobilization density of three types of biomolecules.

Sample	PD-H 20-20	PD-H 40-20	PD-H 60-20
^{D}G (mg/cm2)	0.6 ± 0.3	2.1 ± 0.4	0.5 ± 0.1
^{D}I, CH (mg/cm2)	0.9 ± 0.3	1.4 ± 0.2	0.8 ± 0.2
^{D}I, CH/γ-PGA (mg/cm2)	0.7 ± 0.2	0.8 ± 0.4	0.5 ± 0.2
^{D}I, G (mg/cm2)	1.1 ± 0.6	1.2 ± 0.5	0.9 ± 0.3

D_G, graft density, calculated on the weight differences of hexamethyldisilazane films from variations in processing power. ^{D}I, CH, calculate the immobilization density of chitosan; ^{D}I, CH/γ-PGA, calculate the immobilization density of chitosan/poly-γ-glutamic; ^{D}I, G, calculate the immobilization density of gelatin; PD, processing power; H, deposition time. Processing power of cold plasma treats were 20, 40, 60 W. Deposition time was 20 min.

immobilization density of chitosan, chitosan/γ-PGA, and gelatin peaked in the PD-H 40-20 group (1.4, 0.8, and 1.2 mg/cm^2, respectively), suggesting that the immobilization density increased with the graft density.

Thickness of hexamethyldisilazane films

Fig. 4 displays the effect of processing power on hexamethyldisilazane film thickness under 20-min deposition. As the processing power increased from 20 to 40 and 60 W, the film thickness increased from 69 to 84 and 123 nm, respectively. However, a comparison with Fig. 3 revealed that although graft density increased from 0.6 to 2.1 mg/cm^2 as the film thickness increased from 69 to 84 nm, it dropped to 0.5 mg/cm^2 when the film thickness reached 123 nm.

Analysis of surface hydrophilicity–hydrophobicity

The surface hydrophilicity (or hydrophobicity) of the zirconia substrates varied by the surface processing stage. The contact angle between untreated substrates and a water droplet was approximately 52°. After a hexamethyldisilazane film was coated onto the substrates through cold plasma treatment, the contact angle changed.

The results of the immobilization of chitosan, chitosan/γ-PGA, and gelatin indicated that treatment conditions and the type of biomolecule significantly affected the surface hydrophilicity (or hydrophobicity) of the substrates (Table 3).

FTIR of changes in surface functional groups

Fig. 5(a)–(c) present the surface functional group distributions of PD-H 20-20, PD-H 40-20, and PD-H 60-20. Untreated substrates did not exhibit any characteristic peaks. By contrast, the film-coated substrates had the characteristic peak of the Si–C functional group at approximately 790 cm^{-1}; the characteristic peaks of organic silicon–hydrogen functional groups Si-$(CH_3)_1$, Si-$(CH_3)_2$, and Si-$(CH_3)_x$ at approximately 794 and 1260 cm^{-1}; the characteristic peak of functional group Si–O, resulting from silicon–hydrogen

Table 3 Changes in surface hydrophilicity–hydrophobicity at 20-min deposition.

Water Contact Angle (Degree)			
Untreated	52 ± 5		
Sample	PD-H 20-20	PD-H 40-20	PD-H 60-20
PD-hexamethyldisilazane	100 ± 1	97 ± 2	99 ± 1
$^{O}2^{-Plasma}$	<10	<10	<10
S-grafted AAc	42 ± 3	57 ± 2	40 ± 2
Immobilized CH	25 ± 3	32 ± 3	20 ± 2
Immobilized RCH	38 ± 2	40 ± 1	23 ± 2
Immobilized G	35 ± 1	38 ± 2	20 ± 1

PD-hexamethyldisilazane, a hexamethyldisilazane film was coated onto the substrates through cold plasma treatment; $^{O}2^{-Plasma,}$ O_2 plasma activated on the substrates which had been coated with a hexamethyldisilazane film; S-grafted AAc, substrates were grafted polymerization in the prepared acrylic acid (AAc) solution; Immobilized CH, fixing chitosan biomolecule films; Immobilized RCH, fixing a chitosan/poly-γ-glutamic acid biomolecule film; Immobilized G, fixing gelatin biomolecule films; PD, processing power; H, deposition time. Processing power of cold plasma treats were 20, 40, 60 W. Deposition time was 20 min.

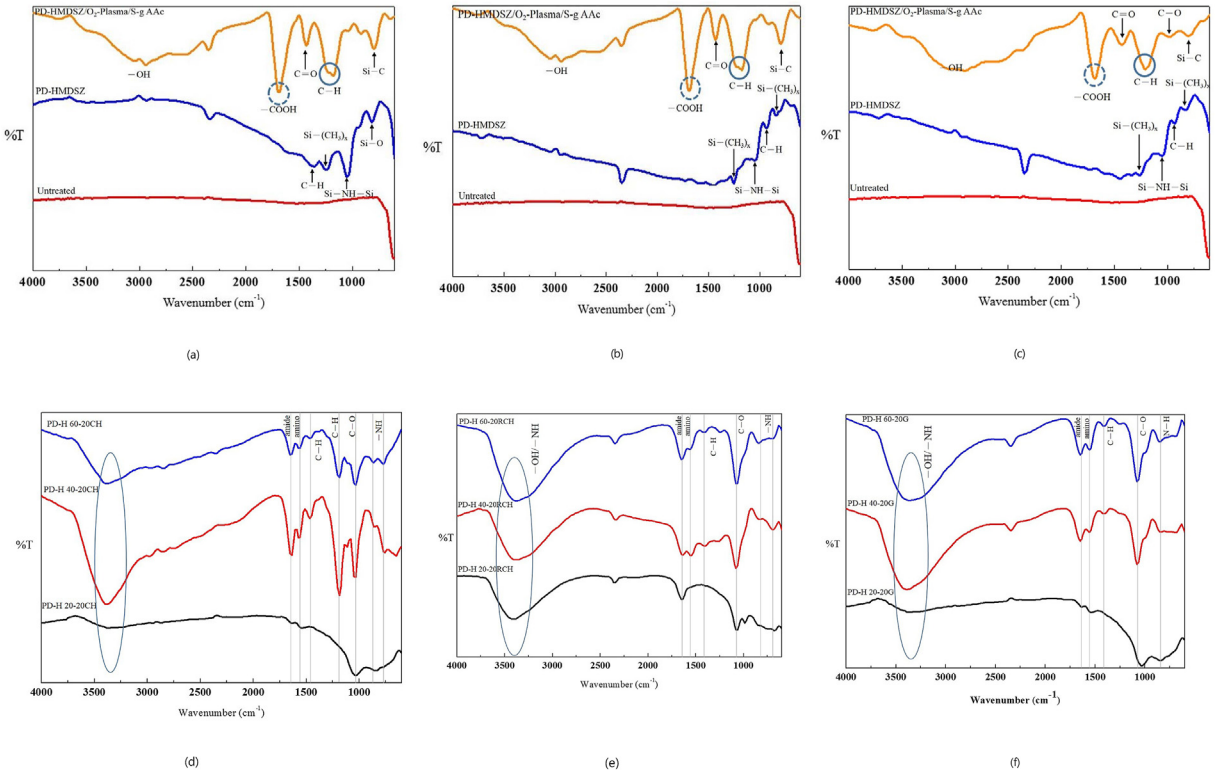

Fig. 5 (a) Surface functional group distribution of PD-H 20-20. (b) Surface functional group distribution of PD-H 40-20. (c) Surface functional group distribution of PD-H 60-20. (d) Surface functional group distribution of immobilized chitosan. (e) Surface functional group distribution of immobilized chitosan/acter. (f) Surface functional group distribution of immobilized gelatin.

compounds being exposed to air, at approximately 800 cm^{-1}; and the characteristic peak of functional group Si—NH—Si at approximately 900—1180 cm^{-1}. The substrates further grafted with polymeric AAc biomolecules exhibited the characteristic peaks of functional groups C—O and C=O at approximately 900—1100 and 1500 cm^{-1}, respectively, and the characteristic peak of functional group —COOH at approximately 1680 cm^{-1}. The characteristic peak of —OH spanned a wide frequency range. All these characteristic peaks represent chemical bonds observable in polymeric AAc molecules.[17]

Fig. 5(d)—(f) present the changes in surface functional groups following the immobilization of chitosan, chitosan/γ-PGA, and gelatin. They provide decisive evidence of interaction between carboxyl groups and amino groups on substrate surfaces. Specifically, the characteristic peak of the amino group, the functional group formed by coexisting —COOH and $-NH_2$, was located at approximately 1599 cm^{-1}. The characteristic peak of the amide group, the functional group formed by the condensation reaction between —COOH and $-NH_2$, appeared at approximately 1648 cm^{-1}; the characteristic peak of was found at approximately 3000 cm^{-1}; and the characteristic peaks of —NH were detected at approximately 665—910 and 3400 cm^{-1}. Regarding —OH, its characteristic peak was prominent, spanning a wide frequency range between 3000 and 3400 cm^{-1}. These results demonstrated that the substrates became hydrophilic following biomolecule immobilization.[18—20]

The changes in immobilization density, surface hydrophilicity—hydrophobicity, and surface functional groups confirmed the successful immobilization of biomolecules on the zirconia substrate surfaces.

MTT assay of MG-63 cell compatibility

Following immobilization of the biomolecules and the culture of MG-63 cells, the PD-H 20-20, PD-H 40-20, and PD-H 60-20 substrates underwent the MTT assay (Fig. 7), with

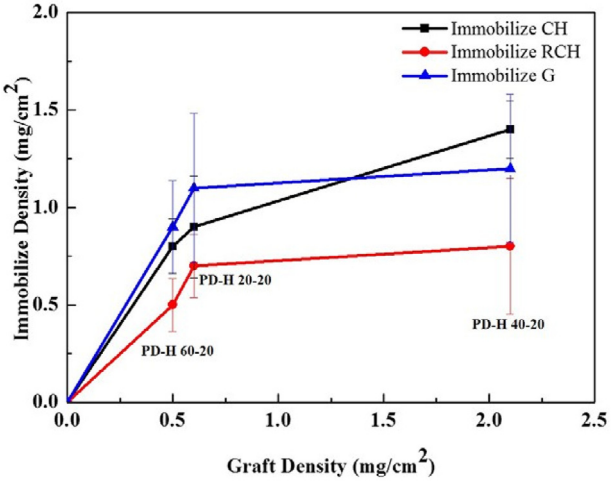

Fig. 6 Relationship between graft density and immobilization density.

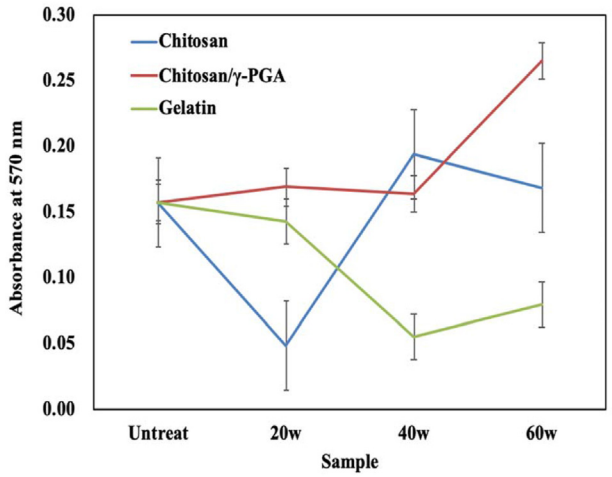

Fig. 7 Changes in light absorbance of immobilized chitosan, chitosan/γ-PGA, and gelatin.

untreated substrates serving as controls. The light absorbance value represented the number of MG-63 cells, thus indicating the viability of MG-63 cells following surface modification and the compatibility of those cells with the surface-modified zirconia substrates.

Discussion

After a hexamethyldisilazane film was deposited, the surface of the substrates became hydrophobic; the contact angle of the water droplets increased from 52° (untreated substrates) to approximately 100° (Table 3). This confirms the observation made in another study that hexamethyldisilazane films are hydrophobic.[21]

The O_2 plasma treatment following film deposition turned the substrate surface ultrahydrophilic, with a contact angle of $<10°$. A possible explanation for this change is that the temporary presence of peroxide groups and —OH was conducive to the graft polymerization of liquid-state polymeric monomers because it enabled the monomers to be evenly distributed on the substrate surface.

Plasma deposition is primarily affected by the processing power and deposition time.[20] When the deposition time is overly long, the chemical bonds on the monomer surfaces constantly break down and reform, and the Si—CH_3 bonds in silicon—hydrogen compounds break into —CH_3, thus reducing the free radicals on the monomer surfaces and lowering the graft density. In other words, the film quality does not necessarily improve as the deposition time increases. Under 20-min deposition, changing the processing power from 20 to 40 and 60 W increased the film thickness from 69 to 84 and 123 nm, respectively. However, although the graft density rose from 0.6 to 2.1 mg/cm^2 as the film thickness grew from 69 to 84 nm, it dropped to 0.5 mg/cm^2 when the film thickness reached 123 nm. This confirms the premise that under an excessively high processing power, the Si—CH_3 bond in silicon—hydrogen compounds can break into —CH_3, reducing the free radicals on the monomer surfaces and lowering the AAc—graft density.[22]

The immobilization density of chitosan, chitosan/γ-PGA, and gelatin all exhibited considerable changes (Table 2). In the PD-H 40-20 condition, their immobilization density peaked at 1.4, 0.8, and 1.2 mg/cm^2, respectively, suggesting that the immobilization density increased with the graft density. When numerous polymeric AAc biomolecules were clustered on the substrate surfaces through graft polymerization, the —COOH groups they contained promoted the condensation reaction involving amino groups in chitosan and gelatin, creating more amide groups. When the graft density increased from 0.5 to 0.6 and then 2.1 mg/cm^2, the curves corresponding to the immobilized chitosan and gelatin became less steep. This indicates the saturation of the substrate surfaces with —COOH groups and amino groups from biomolecules (Fig. 6). The graft density of chitosan/γ-PGA was consistently lower than that of the chitosan and gelatin. This suggested that when the immobilized chitosan was used to produce amide groups, the density of the reaction points (amino groups) was lower than those in chitosan and gelatin (in which —COOH groups were the reaction points). However, when chitosan reacted with γ-PGA, fewer chitosan/γ-PGA nanoparticles than chitosan and gelatin nanoparticles could be immobilized because of the reduced number of active sites.

The immobilization density and surface hydrophilicity—hydrophobicity of chitosan, chitosan/γ-PGA, and gelatin were compared (Table 3). In all three types of biomolecules, when the immobilization density increased, the contact angle also increased, confirming the variation of surface hydrophilicity—hydrophobicity with the immobilization density.

The MTT assay revealed that regarding the immobilized chitosan, MG-63 cells survived in the PD-H 20-20CH, PD-H 40-20CH, and PD-H 60-20CH conditions. After 24 h of cell culture, the biocompatibility of the treated substrates became higher than that of the untreated substrates.

Regarding immobilized chitosan/γ-PGA, the light absorbance values of PD-H 20-20RCH, PD-H 40-20RCH, and PD-H 60-20RCH suggest a biocompatibility comparable to or greater than that of untreated substrates. By contrast, in the case of immobilized gelatin, light absorbance was low in all conditions except for that of PD-H 20-20G, possibly because immobilized gelatin made the substrate surface unsuited to the growth of MG-63 cells. In other words, biocompatibility was poor. Overall, the results suggest that processing power, deposition time, and the type of biomolecule to be immobilized can all critically affect biocompatibility.

This study investigated the optimal graft density for the surface modification of immobilized biomolecules, which involved coating substrates with hexamethyldisilazane films as well as applying cold plasma treatment under varying processing power and deposition time settings. This was followed by the grafting of AAc biomolecules (chitosan, chitosan/γ-PGA, and gelatin) through O_2 plasma and UV-light treatments. A cell compatibility analysis determined that chitosan and chitosan/γ-PGA enhanced zirconia substrates' compatibility with MG-63 cells, whereas gelatin decreased it.

Our findings confirm that cold plasma treatment and graft polymerization can promote the immobilization of

biomolecules and change the biocompatibility of zirconia ceramics. This approach can be applied to the modification of zirconia ceramic implants; therefore, it merits further investigation.

Conflict of Interest

The authors have no conflicts of interest relevant to this article.

Acknowledgments

The study was supported in great part and English editing arrangement by Research Promotion Center,Office of Research and Development, Taipei Medical University, Taiwan.

References

1. Özkurt Z, Kazazoğlu E. Zirconia dental implants: a literature review. *J Oral Implantol* 2011;37:367—76.
2. Borgonovo AE, Censi R, Vavassori V, Arnaboldi O, Maiorana C, Re D. Zirconia implants in esthetic areas: 4-year follow-up evaluation study. *Int J Dent* 2015;2015:415029.
3. Comisso I, Arias-Herrera S, Gupta S. Zirconium dioxide implants as an alternative to titanium: a systematic review. *J Clin Exp Dent* 2021;13:e511—9.
4. Marti A. Inert bioceramics (Al_2O_3, ZrO_2) for medical application. *Injury* 2000;31(Suppl 4):33—6.
5. Maccauro G, Iommetti PR, Raffaelli L, Manicone PF. Biomaterials applications for nanomedicine. In: Pignatello R, ed. *Alumina and zirconia ceramic for orthopaedic and dental devices*. London: IntechOpen, 2011:299—308.
6. Wenz HJ, Bartsch J, Wolfart S, Kern M. Osseointegration and clinical success of zirconia dental implants: a systematic review. *Int J Prosthodont (IJP)* 2008;21:27—36.
7. Hanawa T. Zirconia versus titanium in dentistry: a review. *Dent Mater J* 2020;39:24—36.
8. Bona AD, Pecho OE, Alessandretti R. Zirconia as a dental biomaterial. *Materials* 2015;8:4978—91.
9. Cionca N, Hashim D, Mombelli A. Zirconia dental implants: where are we now, and where are we heading? *Periodontol* 2017;73:241—58.
10. Pieralli S, Kohal RJ, Jung RE, Vach K, Spies BC. Clinical outcomes of zirconia dental implants: a systematic review. *J Dent Res* 2017;96:38—46.
11. Wang SF, Yang TCK, Hsu YT, Lee SY, Yang JC. The structure-property-processing relationship for sintered yttria-stabilized zirconia (YSZ)/alumina bioceramics. *Biomed Eng- Appl Basis Commun* 2013;25:1350005.
12. Siddiqi A, Khan AS, Zafar S. Thirty years of translational research in zirconia dental implants: a systematic review of the literature. *J Oral Implantol* 2017;43:314—25.
13. Wang SF, Yang CK, Yang JC, Lee SY. *Method of surface treatment for zirconia dental implants*. 2014. US8883032 B2.
14. Kuo TF, Lu HC, Tseng CF, Yang JC, Wang SF, Yang TC-K. Evaluation of osseointegration in titanium and zirconia-based dental implants with surface modification in a miniature pig model. *J Med Biol Eng* 2017;37:313—20.
15. Duske K, Koban I, Kindel E, et al. Atmospheric plasma enhances wettability and cell spreading on dental implant metals. *J Clin Periodontol* 2012;39:400—7.
16. Wagner G, Eggers B, Duddeck D, et al. Influence of cold atmospheric plasma on dental implant materials - an in vitro analysis. *Clin Oral Invest* 2022;26:2949—63.
17. Chou HC, Yan TR, Chen KS. Detecting cells on the surface of a silver electrode quartz crystal microbalance using plasma treatment and graft polymerization. *Colloids Surf, B* 2009;73:244—9.
18. Olad A, Azhar FF. The synergetic effect of bioactive ceramic and nanoclay on the properties of chitosan—gelatin/nanohydroxyapatite—montmorillonite scaffold for bone tissue engineering. *Ceram Int* 2014;40:10061—72.
19. Staroszczyk H, Sztuka K, Wolska J, Wojtasz-Pająk A, Kołodziejska I. Interactions of fish gelatin and chitosan in uncrosslinked and crosslinked with EDC films: FT-IR study. *Spectrochim Acta Mol Biomol Spectrosc* 2014;117:707—12.
20. Bukzem AL, Signini R, Dos Santos DM, Lião LM, Ascheri DP. Optimization of carboxymethyl chitosan synthesis using response surface methodology and desirability function. *Int J Biol Macromol* 2016;85:615—24.
21. Carvalho ATD, Carvalho RAM, Silva MLPD, Demarquette N. Hydrophobic plasma polymerized hexamethyldisilazane thin films: characterization and uses. *Mater Res* 2006;9:9—13.
22. Zanini S, Riccardi C, Orlandi M, et al. Surface properties of HMDSO plasma treated polyethylene terephthalate. *Surf Coat Technol* 2005;200:953—7.